Room-Temperature Stimulated Emission and Lasing in Recrystallized Cesium Lead Bromide Perovskite Thin Films

Neda Pourdavoud, Tobias Haeger, Andre Mayer, Piotr Jacek Cegielski, Anna Lena Giesecke, Ralf Heiderhoff, Selina Olthof, Stefan Zaefferer, Ivan Shutsko, Andreas Henkel, David Becker-Koch, Markus Stein, Marko Cehovski, Ouacef Charfi, Hans-Hermann Johannes, Detlef Rogalla, Max Christian Lemme, Martin Koch, Yana Vaynzof, Klaus Meerholz, Wolfgang Kowalsky, Hella-Christin Scheer, Patrick Görrn, and Thomas Riedl*

Cesium lead halide perovskites are of interest for light-emitting diodes and lasers. So far, thin-films of CsPbX₃ have typically afforded very low photoluminescence quantum yields (PL-QY < 20%) and amplified spontaneous emission (ASE) only at cryogenic temperatures, as defect related nonradiative recombination dominated at room temperature (RT). There is a current belief that, for efficient light emission from lead halide perovskites at RT, the charge carriers/excitons need to be confined on the nanometer scale, like in CsPbX₃ nanoparticles (NPs). Here, thin films of cesium lead bromide, which show a high PL-QY of 68% and low-threshold ASE at RT, are presented. As-deposited layers are recrystallized by thermal imprint, which results in continuous films (100% coverage of the substrate), composed of large crystals with micrometer lateral extension. Using these layers, the first cesium lead bromide thin-film distributed feedback and vertical cavity surface emitting lasers with ultralow threshold at RT that do not rely on the use of NPs are demonstrated. It is foreseen that these results will have a broader impact beyond perovskite lasers and will advise a revision of the paradigm that efficient light emission from CsPbX₃ perovskites can only be achieved with NPs.

Metal-halide perovskite semiconductors are of tremendous interest for a variety of applications. Only recently, solar cells based on a representative of this family have been certified with an efficiency in excess of 24%.[1] Aside from their remarkable success in photovoltaics, metal-halide perovskites are also highly promising as light emitters, e.g., in light-emitting diodes (LEDs) or lasers.[2–4] LEDs based on the fruit-fly of these compounds, i.e., methylammonium lead iodide (CH₃NH₃PbI₃ or MAPbI₃), and other related perovskites have been demonstrated with continuously increasing efficiency.[5–7] For lasers, there is the vision that perovskites may overcome/avoid the typical limitations and loss mechanisms present in organic gain media, such as triplet–singlet annihilation or absorption due to triplet excitons and

N. Pourdavoud, T. Haeger, Dr. R. Heiderhoff, Prof. T. Riedl
Institute of Electronic Devices
University of Wuppertal
Rainer-Gruenter-Str. 21, 42119 Wuppertal, Germany
E-mail: t.riedl@uni-wuppertal.de

Dr. A. Mayer, I. Shutsko, A. Henkel, Prof. H.-C. Scheer, Prof. P. Görrn
Chair of Large Area Optoelectronics
University of Wuppertal
Rainer-Gruenter-Str. 21, 42119 Wuppertal, Germany

P. J. Cegielski, Dr. A. L. Giesecke, Prof. M. C. Lemme
AMO GmbH
Otto-Blumenthal-Straße 25, 52074 Aachen, Germany

P. J. Cegielski, Prof. M. C. Lemme
Elektrotechnik und Informationstechnik
Lehrstuhl für Elektronische Bauelemente
RWTH Aachen University
Otto-Blumenthal-Straße 25, 52074 Aachen, Germany

Dr. S. Olthof, Prof. K. Meerholz
Department of Chemistry
University of Cologne
Luxemburger Straße 116, 50939 Cologne, Germany

Dr. S. Zaefferer
Max-Planck-Institut für Eisenforschung
Max-Planck-Str. 1, 40237 Düsseldorf, Germany

D. Becker-Koch, Prof. Y. Vaynzof
Kirchhoff-Institut für Physik
Ruprecht-Karls-Universität Heidelberg
Im Neuenheimer Feld 227, 69120 Heidelberg, Germany

D. Becker-Koch, Prof. Y. Vaynzof
Center for Advanced Materials
Ruprecht-Karls-Universität Heidelberg
Im Neuenheimer Feld 225, 69120 Heidelberg, Germany

M. Stein, Prof. M. Koch
Fachbereich Physik
Philipps-Universität Marburg
Renthof 5, 35032 Marburg, Germany

M. Cehovski, O. Charfi, Dr. H.-H. Johannes, Prof. W. Kowalsky
Institut für Hochfrequenztechnik
Technische Universität Braunschweig
Schleinitzstr. 22, 38106 Braunschweig, Germany

M. Cehovski, O. Charfi, Dr. H.-H. Johannes, Prof. W. Kowalsky
Cluster of Excellence PhoenixD (Photonics, Optics,
and Engineering – Innovation Across Disciplines)
Welfengarten 1, 30167 Hannover, Germany

Dr. D. Rogalla
RUBION
Ruhr-University Bochum
D-44801 Bochum, Germany

polarons.[8–10] Thus, perovskites currently seed a new promise for the realization of electrically operated laser diodes that can be prepared from solution at low temperatures on virtually any substrate. The marriage of perovskite active materials with silicon (nitride) photonics holds promise to unlock substantial progress in the field of integrated optoelectronics.[11,12] Perovskite lasers also bear the potential to cover the spectral region between 530 and 610 nm, known as the "green-gap,"[13] which is difficult to address at room temperature with established inorganic semiconductor gain media, such as indium-gallium-nitride (InGaN) or aluminum-gallium-indium-phosphide (AlGaInP).

Amplified spontaneous emission (ASE) and optically pumped lasing have been reported for $MAPbI_3$ and other hybrid organic–inorganic lead halide perovskites.[14–19] As a result of the soft nature of this class of materials, photonic resonator structures can be directly patterned into $MAPbX_3$ (X = Br, I) by thermal nanoimprint to achieve low-threshold optically pumped perovskite lasers.[20,21]

Unfortunately, MA-based organic–inorganic halide perovskites lack intrinsic stability.[22,23] For improved thermodynamic stability, the volatile organic moiety can be replaced with inorganic cations, such as Cs.[24,25] The corresponding all-inorganic perovskite semiconductors, i.e., cesium lead halides, have been identified as particularly promising for light-emitting applications.[26]

However, early attempts to use thin-films of $CsPbX_3$ for light emission only led to disappointing results with very low photoluminescence quantum yields (PL-QY) of about 16%.[27] More detrimentally, ASE in $CsPbX_3$ thin-films has only been achieved at cryogenic temperatures below 150 K.[28] The poor performance at higher temperatures has been attributed to nonradiative recombination associated with a high number of defects. It must be noted that the $CsPbBr_3$ thin films used in the above studies showed poor film formation and contained a high number of pinholes. Some attempts to improve on film formation and to mitigate the impact of defects were based on blending the perovskite with additives, such as ZnO nanoparticles[29] or thiocyanate ethyl acetate.[30] However, the luminescence quantum yield could not be increased beyond 20% in these reports. Recently, two-photon pumped ASE has been reported in $CsPbBr_3$ single crystals, albeit at relatively high threshold levels (0.65 mJ cm^{-2}, 35 fs pulse width).[31]

Unlike the case of thin films, $CsPbX_3$ nanoparticles (size < 10 nm) or nanorods showed a high PL-QY and exhibited ASE at room temperature.[32–34] Unfortunately, nanosized grains of lead-halide perovskites have been evidenced to be subject to serious stability issues.[35] Moreover, stabilizing and solubilizing capping ligands are typically required, that not only deteriorate charge transport but may likewise impede thermal transport, which is a particular problem for lasers, especially if electrical and/or continuous wave operation is considered.[36–38] Nevertheless, the impressive results achieved with $CsPbX_3$ nanoparticles nurtured the paradigm that for efficient light emission from lead halide perovskites at room temperature, one needs to confine the charge carriers/excitons on the nanometer scale to prevent their migration to nonradiative defects.[5,39]

Here, we present results that challenge this paradigm. We demonstrate thin films of cesium lead bromide, which show a high photoluminescence quantum yield of 68% and ASE at room temperature with low threshold. The continuous films

(≈100% coverage of the substrate) are composed of large crystals with micrometer lateral extension. Our layers result from originally rough as-deposited layers, which were recrystallized by thermal imprint. Using these layers, we demonstrate the first cesium-lead bromide thin-film distributed feedback (DFB) and vertical cavity surface emitting lasers (VCSELs) with ultralow threshold at room temperature, that do not rely on the use of nanoparticles. Our results render this all-inorganic gain medium an excellent material platform for perovskite laser diodes in the future. We also foresee that our results will have a broader impact beyond perovskite lasers and will possibly lead to a revision of the belief that efficient light emission from $CsPbX_3$ perovskites could only be achieved with nanoparticles.

The cesium lead bromide thin films used in this study have been prepared from a solution of cesium bromide (CsBr) and lead bromide ($PbBr_2$) in dimethylsulfoxide (DMSO). The molar ratio of $CsBr:PbBr_2$ was varied between 0.5:1 and 3:1. Initially, a ratio of 1:1 was chosen. The as-deposited layers were recrystallized by a thermal imprint process at 150 °C and a pressure of 100 bar, using a flat piece of silicon wafer as stamp (**Figure 1**a). More details about the film deposition and the thermal imprint process can be found in the Experimental Section.

The as-deposited solution processed cesium lead bromide films are very rough (roughness 23.8 nm, rms) and show a considerable number of pin-hole defects (Figure 1b). The external photoluminescence quantum yield (PL-QY) (η_{ext}) at RT is about 9.3%. This η_{ext} can be translated to an internal PL-QY (η_{int}) of about 43% (see the Supporting Information for details of the determination of η_{int} taking a limited outcoupling probability into account[40]). It is important to note, that with these layers we were not able to achieve amplified spontaneous emission (ASE) at room temperature, even under pulsed excitation at levels of 600 μJ cm^{-2} (λ = 355 nm, pulse duration ≈300 ps), which already marks the onset at which the focused laser beam starts to machine the perovskite thin film. Upon recrystallization by thermal imprint, the layers change strikingly. The layers become very smooth (roughness: 0.5 nm, rms) and are composed of large crystals with micrometer-sized lateral dimensions (Figure 1c). Photographs of pristine and pressed layers (on silicon) clearly demonstrate the mirror-like surface of the pressed layers as opposed to the dull impression of the rough pristine layer. The time resolved analysis of the PL decay dynamics is shown in Figure 1e. The data are fitted by a biexponential decay. For the pristine sample, decay times of τ_1 = 4.1 ns and τ_2 = 10 ns are determined. In the recrystallized layers a notable increase of τ_1 = 5.9 ns and τ_2 = 19 ns is found, which are similar to decay times reported for $CsPbBr_3$ single crystals.[41–43] The PL spectra for pristine and pressed layers are shown in Figure 1f. Most notably, the spectral width (full-width half-maximum) is substantially reduced from $\Delta\lambda$ = 20.1 nm ($\Delta(h\nu)$ = 91 meV) for the pristine layer to 14.5 nm (66 meV) for the pressed layer. Note, while the short-wavelength edge of the PL spectra is very similar, the high-wavelength edge is significantly redshifted in the pristine layers, which indicates recombination via near-band-edge defects.[44] As such, the narrowed PL linewidth supports the conclusion of an overall improved material quality in the pressed layers.

Notably, η_{int} of the recrystallized films increased to 53%. In strong contrast to the pristine layers, the recrystallized
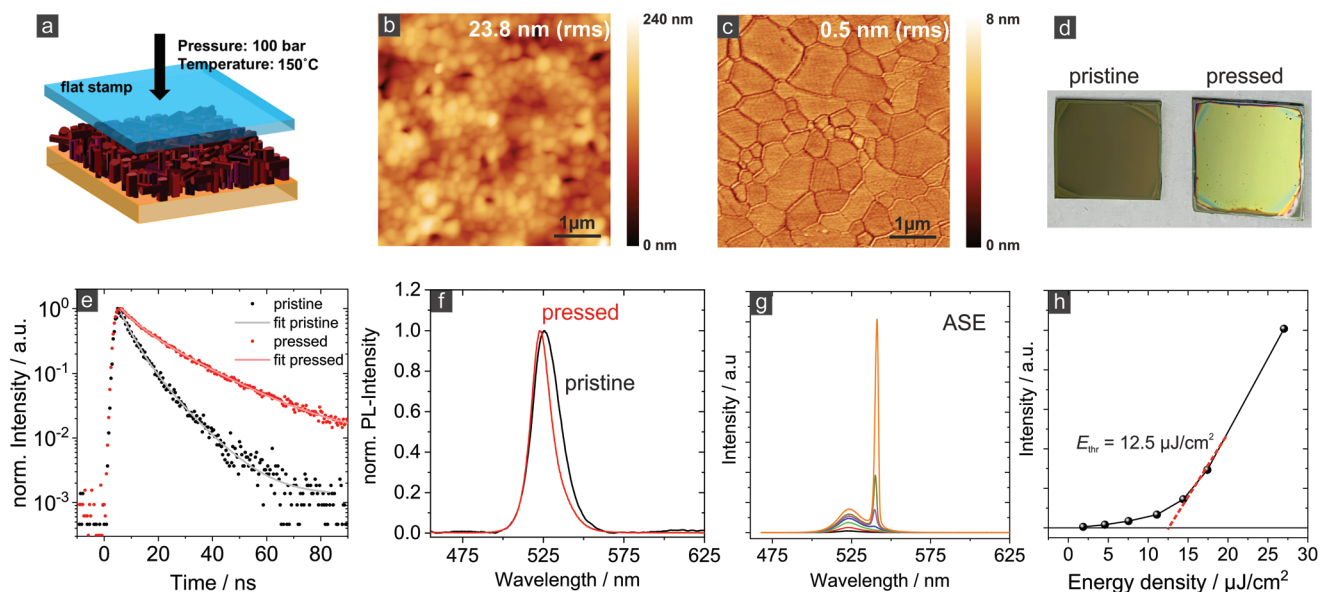
1903717 (2 of 10)

Figure 1. a) Schematic of the thermal imprint process using a flat silicon stamp to recrystallize the as-deposited cesium lead bromide layer. b,c) Atomic force microscopy of layers before (b) and after (c) thermal imprint. The layer thickness is 120 nm. d) Photograph of pristine and pressed layers on silicon substrate. e,f) Time-resolved photoluminescence (PL) decay and PL spectra for pristine (black) and pressed (red) layers at room temperature. Amplified spontaneous emission measurement on a flattened cesium lead bromide thin-film: g) emission spectra and h) corresponding output characteristics.

films show ASE at room temperature (λ_{ASE} = 541 nm, spectral width ≈2.5 nm) under pulsed excitation with a low threshold of 12.5 µJ cm^{-2} (Figure 1g,h).

Taken together, the optical analysis revealed an improved PL-QY and an increased PL lifetime in the recrystallized layers. An increasing grain size in halide perovskite layers has been reported to infer an increased PL lifetime.[45] The finding has been explained by a decreasing radiative rate for larger grains due to the concomitantly decreasing bandgap. Note, we did not observe a similar variation of the bandgap in our films (Figure 1f). On the other hand, de Quilettes et al. provided evidence for the substantial importance of nonradiative recombination at grain boundaries in halide perovskite thin films.[46] The latter result together with the concomitantly observed increase of the PL-QY indicate an effective mitigation of nonradiative recombination in our recrystallized samples, being the key for achieving ASE at room temperature.

To further characterize the structural properties of our samples, we measured the X-ray diffractograms for pristine and pressed layers (**Figure 2**a,b). The pristine sample exclusively shows reflections attributed to the orthorhombic CsPbBr$_3$ phase (ICSD 97851), with a minor peak at 18.62°, which could be due to PbBr$_2$. In striking contrast, the pressed and recrystallized film shows two orders of magnitude more intense peaks, that can be assigned to the tetragonal 2D phase CsPb$_2$Br$_5$ (i4mcm, JCPDS No. 025–0211, Figure 2b). The dominance of the 002, 004, 006, 008 peaks indicates the high degree of orientation of the crystals, which is also evidenced by electron backscatter diffraction (EBSD) (see Figure S1, Supporting Information). However, it has to be noted that in the pressed layers the reflections due to the 3D CsPbBr$_3$ phase have also gained by a factor of three in intensity compared to the pristine layer (see inset Figure 2b). As such, X-ray diffraction (XRD) provides evidence of substantial recrystallization and an overall improved crystal

quality upon thermal imprint. We have also studied the resulting layers by photothermal deflection spectroscopy and THz absorption spectroscopy (Figure S2). The energy gap derived from the absorption spectra is E_g = 2.32 eV (534 nm) for both the pristine and the pressed layer, corresponding to the direct bandgap of CsPbBr$_3$. For CsPb$_2$Br$_5$ an indirect bandgap of 3 eV or larger has been reported.[47,48] The Urbach energy of the recrystallized layer is 17.4 meV, similar to what has been reported for high-quality CsPbBr$_3$ single crystals[41] and substantially lower than that of the pristine film (20.6 meV), suggesting a lower degree of energetic disorder within the recrystallized films and agrees with the narrowed PL-linewidth (Figure 1f). THz absorption spectroscopy conducted at room temperature revealed sharp absorption peaks in the recrystallized layers at 1.025 THz (34 cm^{-1}), 1.428 THz (47.6 cm^{-1}), and 1.965 THz (65.5 cm^{-1}), whereas the spectrum for the pristine layer only shows less-pronounced features at similar positions. These results are indicative of a substantially reduced number of structural defects in the recrystallized layers.[49] The peak positions agree with the energy of lattice vibrations, reported for single crystals of CsPbBr$_3$ and CsPb$_2$Br$_5$.[50,51]

Composites of CsPbBr$_3$ and CsPb$_2$Br$_5$ have recently attracted great attention to improve light emission in nanoparticles and nanoplates.[52,53] The formation of the mixed-phase (CsPbBr$_3$–CsPb$_2$Br$_5$) perovskite upon annealing CsPbBr$_3$ nanoparticle films has been studied by Manna and co-workers.[54,55] In that report, the pristine layers showed a PL-QY of 19% which decreased to <1% after formation of the mixed CsPbBr$_3$–CsPb$_2$Br$_5$ phase.

To elucidate the presence of the 2D and 3D phases in our pressed layers, we performed scanning electron microscopy (SEM) and EBSD (Figure 2c,d). Interestingly, the SEM image obtained with backscattered electrons shows a very pronounced contrast of bright and dark crystals, which cannot be explained
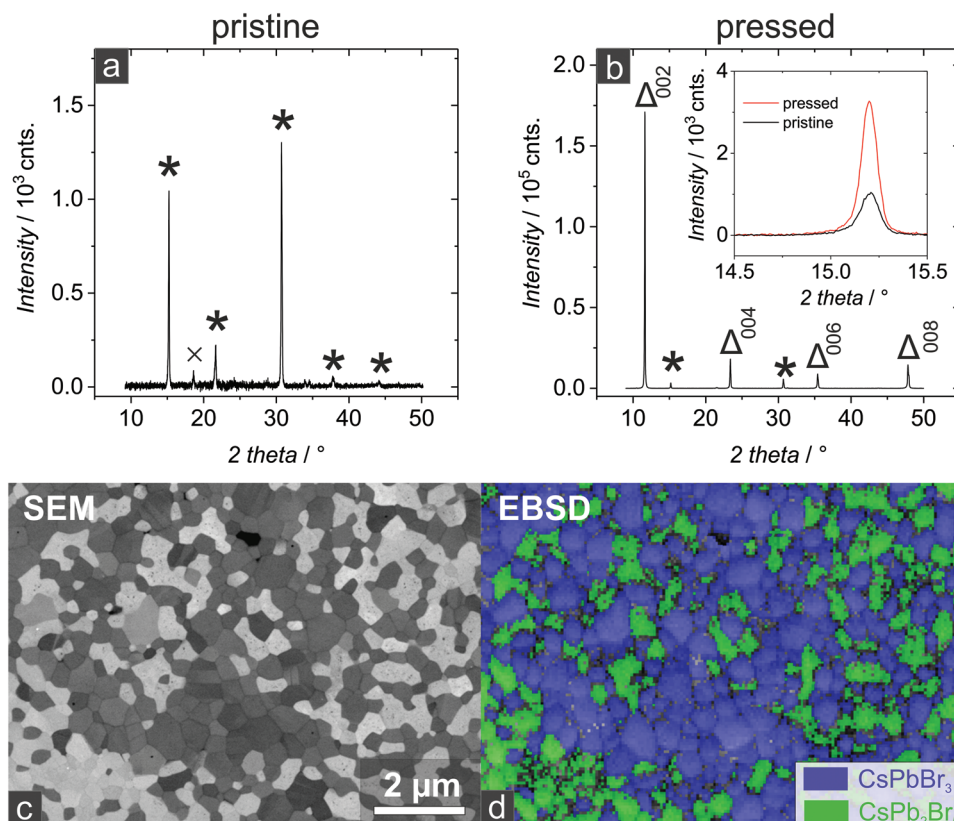
Figure 2. a,b) X-ray diffractograms of pristine (a) and pressed (b) films. The symbols mark diffraction peaks due to $CsPbBr_3$ (∗), $CsPb_2Br_5$ (Δ), and $PbBr_2$ (×). Note, the *y*-axis in (b) spans a two orders of magnitude larger scale than that of (a). The inset compares the 110 diffraction peaks of the orthorhombic $CsPbBr_3$ in the pristine and pressed layer. c) Scanning electron microscopy (SEM) image obtained with backscattered electrons, and d) electron backscatter diffraction (EBSD) of a pressed/recrystallized layer. The assignment of the $CsPbBr_3$ and $CsPb_2Br_5$ has been made on the basis of published crystallographic data (see the Experimental Section).

by topography effects. EBSD reveals that the crystals that appear dark in SEM are $CsPbBr_3$ (3D) while those appearing bright are $CsPb_2Br_5$ (2D) (see the Supporting Information). The higher lead content in the 2D phase is expected to cause stronger scattering of electrons, which accounts for the higher brightness in the backscattered SEM image. The pole figures obtained in EBSD for both $CsPbBr_3$ (3D) and $CsPb_2Br_5$ (2D) show a strong 001 orientation, which is particularly pronounced for the 2D phase. (Figure S1, Supporting Information).

Thermal microscopy has shown a similar contrast associated with the 2D and 3D phase in thermal conductivity.[56] The coexistence of the two phases is further supported by optical transmission/PL microscopy (Figure S3, Supporting Information). PL microscopy shows that the light emission results exclusively from the 3D phase while the 2D parts are nonemissive. This is in contrast to earlier reports that claimed that the formation of $CsPb_2Br_5$ inferred a substantial improvement in PL-QY.[57] According to a quantitative analysis of the SEM images using an image processing software, we can determine the relative content of $CsPb_2Br_5$ to be 46% in these samples.

In order to identify whether and to what extent the presence of the nonemissive 2D phase is beneficial for the light emission of the film, i.e., to passivate defects, we aimed to reduce the formation of $CsPb_2Br_5$ by increasing the concentration of CsBr in the precursor solution. Unfortunately, the solubility

of CsBr in DMSO is limited and precipitates are forming upon increasing the molar content of CsBr. Rutherford backscattering spectrometry (RBS) shows that precursor solutions with a nominal molar ratio of $CsBr:PbBr_2$ ranging from 0.5:1 to 3:1 afford pristine layers with a substantially lower relative Cs content (**Figure 3**a). For example, for $CsBr:PbBr_2 = 1:1$ in the precursor, we find [Pb]/[Cs] = 1.4 and [Br]/[Pb] = 2.7 in the film. Overall, the [Pb]/[Cs] and [Br]/[Pb] ratio determined by RBS is in favorable agreement with the relative abundance of $CsPb_2Br_5$ and $CsPbBr_3$ identified by the bright and dark regions in the SEM images, respectively (see discussion above). Most notably, a ratio of [Pb]/[Cs] = 1 and [Br]/[Pb] = 3 in the film is found for a nominal ratio of $CsBr:PbBr_2 = 2.75:1$ in the precursor. Indeed, XRD clearly shows a gradual reduction of the abundance of the 2D phase relative to that of the 3D phase in the pressed layers prepared with a $CsBr:PbBr_2$ ratio increased from 1:1 to 2.6:1 (Figure 3b). Finally, for $CsBr:PbBr_2 = 2.75:1$ the signal due to the 2D phase is entirely absent and only intense reflections due to the 3D phase are found. In the SEM image taken from the 2.75:1 sample, no bright/dark contrast as in the mixed phase samples is found (Figure S4). To understand how the presence of the 2D phase affects the ASE threshold we studied the samples under pulsed optical excitation at elevated excitation densities. The corresponding ASE threshold is shown in Figure 3c. Most importantly, the ASE threshold remains constant for a
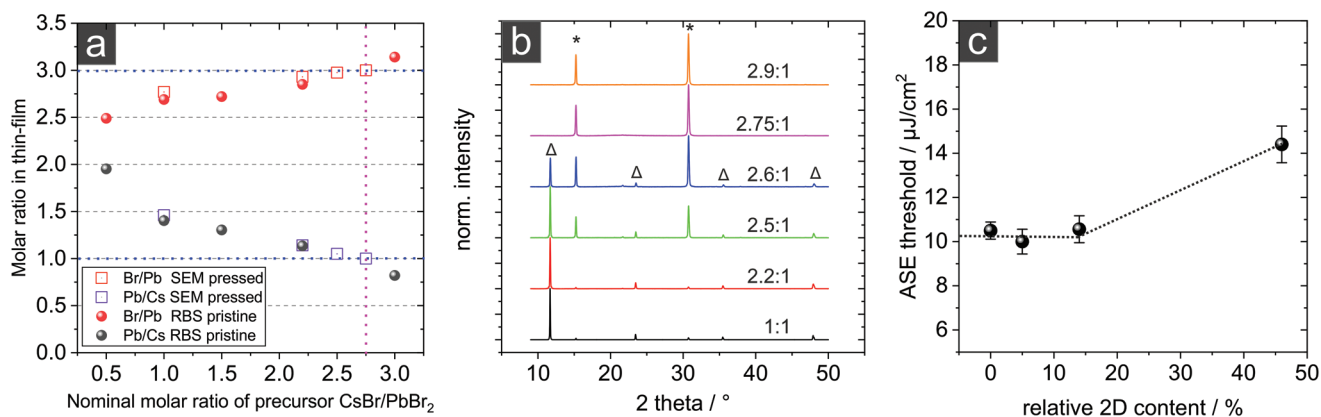
Figure 3. a) Molar ratio Pb/Cs and Br/Pb in the pristine and pressed films versus nominal molar ratio (CsBr/PbBr$_2$) of the precursor. The ratio in the film has been determined by RBS and SEM (see text), respectively. b) X-ray diffractograms of pressed films resulting from a varied CsBr/PbBr$_2$ ratio of the precursor. The symbols mark diffraction peaks due to CsPbBr$_3$ (*), CsPb$_2$Br$_5$ (Δ). c) ASE threshold of pressed films with varied relative content of 2D phase (CsPb$_2$Br$_5$).

relative content of 2D phase in the film below 15%. There is a slightly elevated threshold for layers with a higher 2D content of around 50%. This is in part attributed to a strongly reduced amount of active material, as the wide-gap, indirect 2D-phase does not contribute to the ASE. Note, the internal PL-QY for the purely 3D CsPbBr$_3$ thin-film is found to be 68% (see the Supporting Information for details of the determination of the internal PL-QY taking a limited outcoupling probability into account[40]), higher than the 53% we determined for the mixed phase samples (Figure 1f).

Thus, our results clearly demonstrate that the improved optical properties of the layers are not inferred by the formation of 2D

CsPb$_2$Br$_5$, but rather by the overall improved crystal quality due to recrystallization of the CsPbBr$_3$, which mitigates non-radiative recombination. A further important insight results: Efficient light emission in this class of materials is not exclusively linked to nanocrystals, but room-temperature ASE can likewise be provided by thin films, such as our high-quality recrystallized layers.

In the following we utilize the outstanding optical properties of the recrystallized cesium lead bromide in laser structures. First, we consider DFB resonators. To this end, we employ a stamp with a periodic line pattern (3600 lines mm^{-1}, i.e., periodicity: Λ = 278 nm) for the thermal imprint as schematically shown in **Figure 4**a. The stamp is a commercially
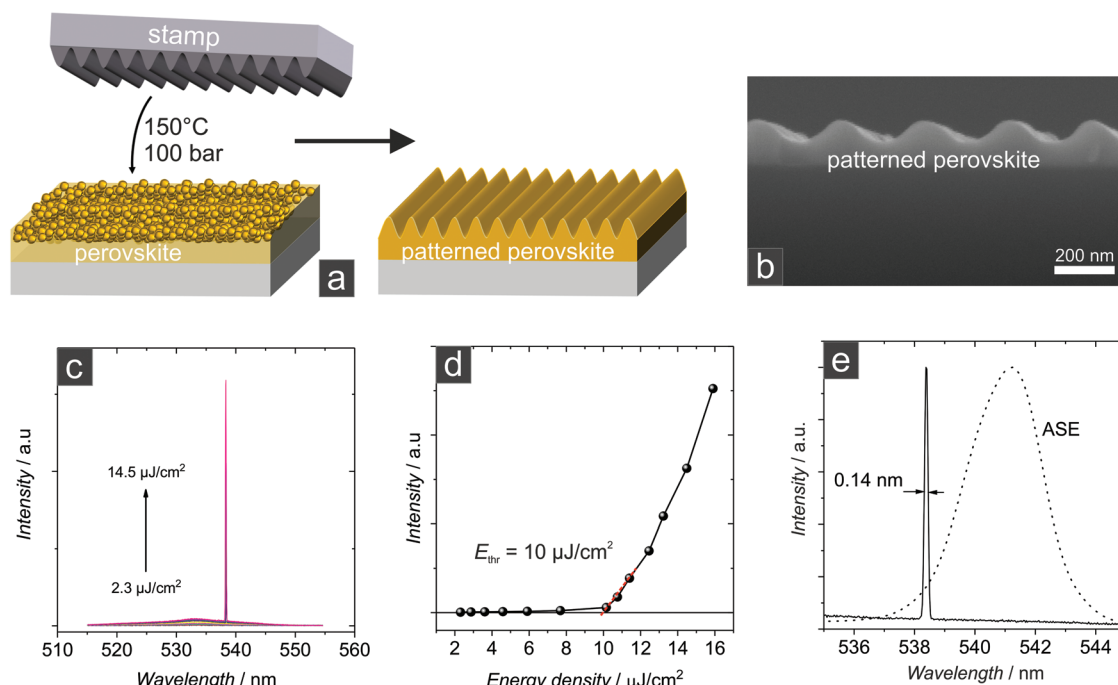

Figure 4. a) Schematic of the direct thermal imprint of a linear grating (periodicity Λ = 278 nm) into the perovskite layer. Glass is used as a substrate. b) SEM image of the cross-section of the patterned perovskite layer. c) Optical emission spectra and d) output intensity upon increasing the pumping energy density. e) High-resolution spectrum of the DFB laser emission line. The ASE spectrum of a flattened layer is shown for comparison (see also Figure 1g).

**ADVANCED
SCIENCE NEWS**

www.advancedsciencenews.com

**ADVANCED
MATERIALS**

www.advmat.de

available diffraction grating (ThorLabs, GH25-36U). The as-casted perovskite layers (on glass substrates) are directly patterned by thermal imprint resulting in a perovskite layer with a sinusoidal grating structure as shown in the SEM image of the cross-section (Figure 4b). Upon pulsed optical pumping, laser emission is found at $\lambda_L = 538.32$ nm above a threshold of 10 μJ cm^{-2} (Figure 4c).

The laser emission is detected perpendicular to the sample surface and the emission spectrum shows a full width at half maximum of 0.14 nm, significantly narrower than the ASE spectrum. The emission wavelength can be understood in the framework of a second order DFB laser, where the Bragg condition is given by $\lambda_L = n_{eff} \times \Lambda$. Accordingly, n_{eff} denoting the effective refractive index of the laser mode is $n_{eff} = 1.938$.

In contrast to the direct patterning of the perovskite layer, we can also use a prepatterned substrate to form a DFB perovskite laser (**Figure 5**). Specifically, glass substrates are coated with a polymer resin (Ormocore, micro resist technology GmbH), which is optically highly transparent and can be patterned by thermal imprint. For the patterning of the Ormocore layer, we again use the diffraction grating as stamp. The perovskite layer is coated on top of these prepatterned substrates and is subsequently recrystallized and flattened by thermal imprint using a flat silicon stamp (Figure 5a). The SEM cross-section image

shows the perfect filling of the grooves of the substrate with the perovskite and the flat surface of the perovskite layer. Upon pulsed optical pumping, lasing can be achieved with a likewise low threshold of 7.2 μJ cm^{-2} (at $\lambda = 539.1$ nm) and narrow linewidth (Figure 5b–d). The inset in Figure 5d shows the dual lobed far-field emission spectrum above threshold, which is characteristic for DFB lasers with predominant complex coupling.[58] As verified in Figure 5e the emission is characterized by a typical strong linear polarization.

Aside from DFB resonators, VCSELs are very attractive for a number of applications, due to their circular beam profile and potentially small footprint. The only all-inorganic perovskite VCSELs reported so far were based on CsPbBr$_3$ nanocrystals as gain medium.[59,60] Here, we employ recrystallized thin films instead to achieve ultralow threshold levels. Specifically, we utilize commercially available dielectric flat mirrors (ThorLabs, FD1M) with transmission characteristics as shown in Figure S5. Importantly, these mirrors show a reflection of up to 99.79% in the spectral region of 530–570 nm. The VCSEL layout in this study is schematically shown in **Figure 6**a.

Briefly, we use one of the dielectric mirrors as a substrate onto which a cesium lead bromide layer is coated. An identical mirror is then used as a stamp for the thermal imprint/recrystallization
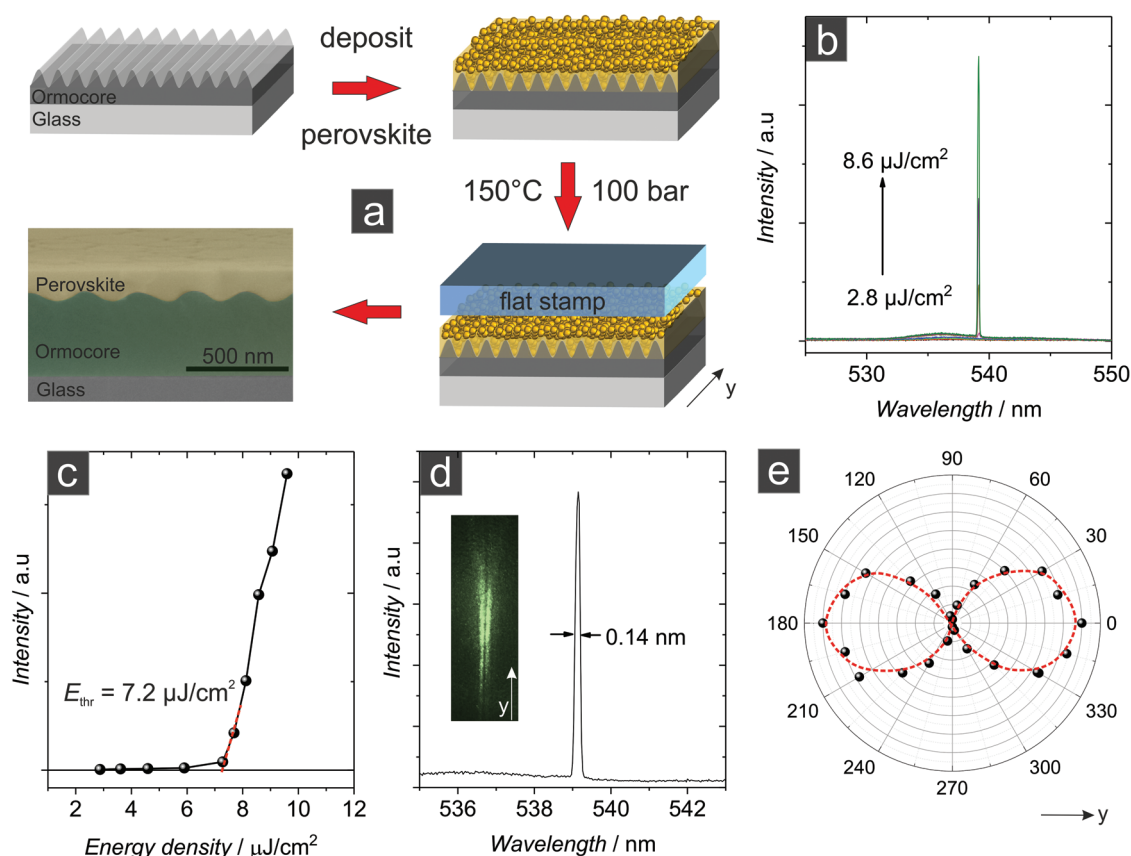

Figure 5. a) Schematic of preparing perovskite DFB laser on a prepatterned carrier. b) Optical emission spectra and c) output intensity upon increasing the pumping energy density. d) High-resolution spectrum of the laser emission line (inset: photograph of the far-field emission profile). e) Polarization characteristics of the second order DFB laser emission. The results shown in this figure and in Figure 4 represent the first all-inorganic CsPbBr$_3$ thin-film distributed feedback lasers. Their low-threshold operation at room temperature is made possible by the recrystallization by thermal imprint.
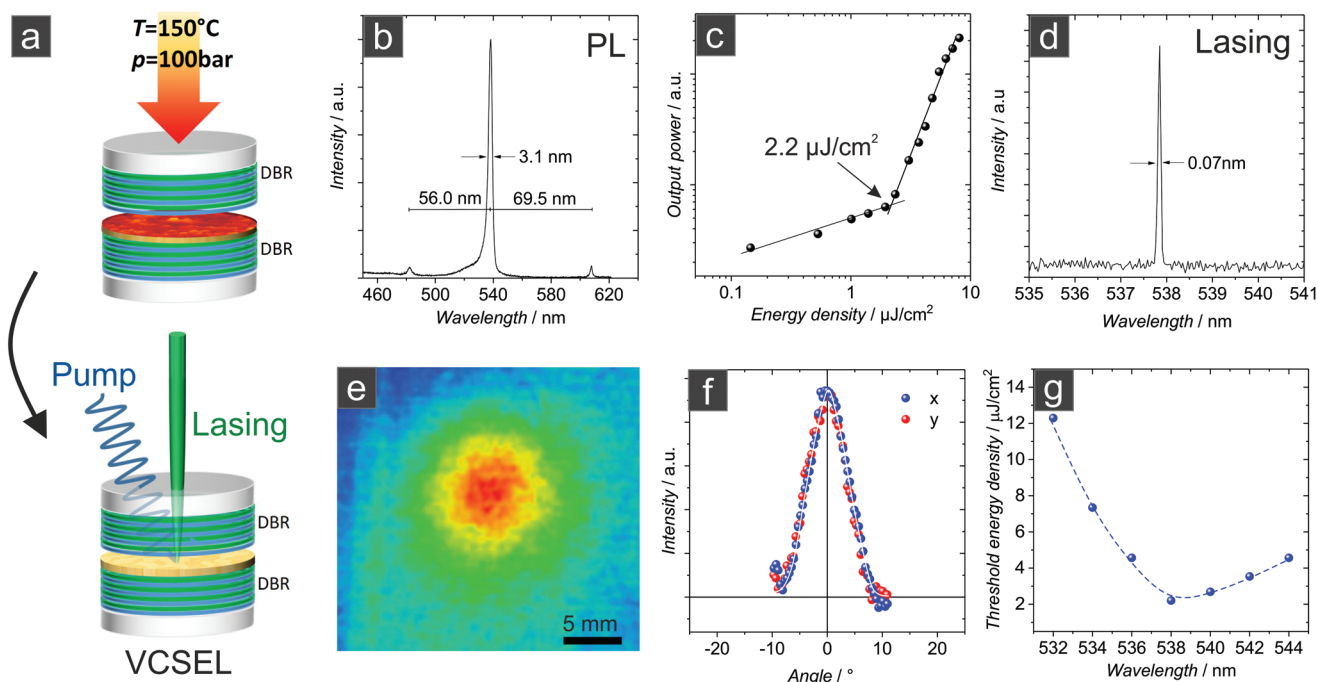
Figure 6. a) Schematic of VCSEL setup. b) Cavity mode spectrum below threshold. c) Output power versus pump energy density. d) Emission spectrum and e,f) far-field beam characteristics of the VCSEL above threshold. The laser beam has been directed on a sandblasted glass screen that had been positioned in a distance of 3 cm from the VCSEL surface. g) Laser threshold energy density in dependence on the emission wavelength.

process (150 °C, 100 bar). Afterward, the stamp is left attached on top of the recrystallized perovskite layer, and the entire assembly forms the VCSEL. Below threshold the luminescence spectrum is characterized by marked resonator modes (Figure 6b). The respective spacing ($\Delta\lambda$) of these modes allows us to derive the effective cavity length $L_{eff} = \lambda^2/(2 \times \Delta\lambda)$ ≈ 2.3 µm. Note, the perovskite layer is about 110 nm thick. Upon pulsed excitation, the VCSEL shows lasing with a threshold of 2.2 µJ cm^{-2}.

Note, for VCSELs based on CsPbBr$_3$ nanocrystals as gain media a threshold of 0.39 µJ cm^{-2} has been reported by Huang et al., albeit upon pumping with fs-pulses.[59] When the authors used ns-pulses instead, they observed an increase of the threshold by more than two orders of magnitude to 98 µJ cm^{-2}. This striking phenomenon was attributed to an increased thermal load under ns-excitation because the thermally insulating shell of the ligands attached to the nanocrystals prevented efficient thermal transport. At the same time, the authors found a decay time of ≈ 10 ps for stimulated emission, which could likewise account for the marked increase of threshold upon ns-pumping. A similar increase of the ASE threshold from 5.3 to 450 µJ cm^{-2} has been found by Yakunin et al. when going from fs- to ns-excitation.[32] The authors explained their finding with the duration of the pump pulse either being substantially shorter or longer compared with the ASE decay time of ≈ 100 ps of the gain medium. Compared to the fs-data in these reports, our CsPbBr$_3$ thin-film VCSELs were pumped with relatively "long" pulses of 300 ps. As such, the low threshold level of 2.2 µJ cm^{-2} for our lasers is therefore even more notable and points to the excellent material quality of the gain medium. The VCSEL emission spectrum is very narrow ($\Delta\lambda = 0.7$ Å,

limit of the spectral resolution of the spectrometer) and the emitted beam shows circular symmetry (Figure 6 e,f). Thanks to a slight (unintentional) variation of the perovskite layer thickness, which leads to some tuning of the resonator length, we were able to likewise tune the laser emission spectrum between $\lambda = 532$–544 nm (Figure 6 g). Note, the reflectance of the DBR mirrors remains essentially unchanged in this region, which is why we can attribute the variation in the threshold energy density to correspond to the spectral shape of the gain spectrum of the active medium.

In summary we have shown highly efficient photoluminescence (PL-QY = 68%), amplified spontaneous emission, and low-threshold lasing in thin-films of cesium lead bromide at room temperature for the first time. Importantly, our layers are not based on nanocrystals or quantum dots but consist of extended continuous layers, which formed upon recrystallization of as-deposited layers by thermal imprint (100 bar, 150 °C). We were able to prepare phase pure 3D CsPbBr$_3$ films, and we provided evidence, that the presence of the 2D CsPb$_2$Br$_5$ phase is not required to render these layers excellent light emitters and active gain media. Building on these recrystallized layers, we demonstrated the first cesium lead bromide thin-film DFB and VCSELs with ultralow threshold (2.2 µJ cm^{-2}, 300 ps pump pulses) at room temperature, that do not rely on the use of nanoparticles. Our results render cesium lead bromide thin-films an excellent material platform for perovskite laser diodes in the future. We also expect that our results will impact perovskite device research beyond lasers and should lead to the revision of the paradigm that efficient room-temperature light emission from CsPbX$_3$ perovskites could only be achieved with nanoparticles.

Experimental Section

Cesium Lead Bromide Layer Preparation: Lead bromide (purity 99.999%, ultradry) (Alfa Aesar) and cesium bromide (99.999%, trace metal basis) (Sigma-Aldrich) were dissolved in anhydrous DMSO with molar ratio of CsBr to $PbBr_2$ varied between 0.5:1 and 3:1 (stirred and heated over night at 60 °C in a nitrogen-filled glovebox). The solution was filtered using a 0.2 µm filter before use.

Borofloat glass substrates were used for the lasers and silicon wafers for SEM, EBSD, and RBS characterization. For PL-QY measurements silicon wafers with 1.5 µm of thermal oxide on top were used. For PDS and THz spectroscopy, quartz substrates were used. All substrates were cleaned by sonication in citric acid, deionized water, and isopropanol (each step 15 min). After drying, the substrates were transferred to a nitrogen-filled glovebox. The perovskite layers were prepared by spin-coating the precursor solution at 4000 rpm, 120 s, and 11 s ramp. After spin-coating, the films were annealed on hotplate at 100 °C for 20 min.

Thermal Nanoimprint and Hot Pressing: Thermal nanoimprint and planar hot pressing experiments were performed in a parallel plate-based imprint system.[61] During heat-up of the system to the processing temperature of 150 °C, which, in this case, took about 20 min, the pressure of 100 bar was applied. When the imprint temperature was reached, the pressure was kept constant for 5 min. Afterward the system was cooled down and the pressure was released slowly as soon as the temperature was below 30 °C. The stamp used for nanoimprint is a commercial diffraction grating (3600 lines mm^{-1}, i.e., periodicity: $\Lambda = 278$ nm, ThorLabs, GH25-36U) and provided with an antisticking layer.[62,63] For the prepatterned gratings Ormostamp (microresist, Berlin) was patterned. For planar hot pressing the stamp was unpatterned silicon, again provided with an antisticking layer. The procedure for planar hot pressing was similar to the imprint procedure; the prepressure used was 100 bar and the pressing time was increased to 30 min. The laser devices were based on the films resulting from a nominal 1:1 molar ratio of CsBr to $PbBr_2$.

Characterization of Materials: XRD was measured using a Panalytical Empyrean system with a Cu Kα anode ($\lambda = 1.54056$ Å). For XRD, layers on glass substrates were used. For the SEM studies layers on Si substrates were investigated using a Philips XL30S FEG microscope with a field emission cathode. AFM measurements were conducted with a Bruker Innova system in tapping mode (tip: RTESPA-300; tip radius: <12 nm).

The microstructure of the material was further studied using EBSD mapping. No specific sample preparation was applied. A Bruker nanosystem with an X-flash EBSD camera, installed on a Zeiss Merlin SEM, was used for the measurements. The measurements were done at 30 kV acceleration voltage and 2 nA beam current. The patterns were binned to 160×120 pixel size and exposed for 30 ms, resulting in a measurement rate of 33 frames per second. The analysis of the measured maps was carried out using the EDAX/TSL software OIM DC. Further details can be found in the Supporting Information.

Absorption spectra were measured by photothermal deflection spectroscopy (PDS). The samples were submerged in an inert liquid (Fluorinert FC-770), which acts as deflecting medium for a probing laser beam (REO R-31008) of 633 nm wavelength and passes parallel to the samples surface. Its deflection, measured by a position sensitive detector (Thorlabs PDP90A) amplified by a lock-in amplifier (Ametec 7230), was directly linked to the absorption of the sample, and caused by the heat created from the absorbed pumping light in the sample. The chopped excitation light was provided by a Xenon arc lamp (Ushio 150W with Abet housing) and a subsequent monochromator.

RBS was performed at the 4 MV tandem accelerator of the RUBION facility (University of Bochum, Germany). A 2 MeV $^4He^+$ ion beam (beam current of 20–40 nA) in combination with a silicon surface barrier detector at an angle of 160° was used.

For photoluminescence (PL) measurements, a laser diode ($\lambda = 450$ nm, power density 0.2 W cm^{-2}) was used. The PL spectra were dispersed in a monochromator (Princeton Instruments, Acton SP2500, gratings: 300 and 1200 lines mm^{-1}) and detected by a thermoelectrically cooled charge coupled device camera (Princeton Instruments).

External PL-QY was measured using a focused continuous wave laser beam (RLDE405M-50-5, Roithner-Lasertechnik, wavelength: 405 nm, power density: 15 W cm^{-2}). As substrates for the perovskite layers Si wafers covered with 1.5 µm thermal SiO_2 were used. The sample was attached to one of the ports of an integrating sphere (RTC-060-SF, Labsphere). The excitation signal was blocked from entering the detector by a filter (03FCG065, Melles Griot) and the PL signal was detected with a power meter (PM100USB, Thorlabs).

The time-resolved PL measurements were done using a Streak camera (Hamamatsu Streak scope C4334). The samples were optically pumped with a Nd:YVO laser (3rd harmonic, wavelength: 355 nm, pulse width: 700 ps, repetition rate: 1 kHz, energy density: 1.5 µJ cm^{-2}). An optical fiber attached to the Streak camera and a lens system collected part of the emitted light from the samples.

The THz absorption spectroscopy was conducted using the output of a 1 kHz titanium-sapphire-based regenerative amplifier system with 35 fs pulses spectrally centered at 800 nm. The output of the amplifier was split into two parts. One part drove a low-temperature grown large aperture Galliumarsenide antenna, which emitted spectrally broad THz pulses ranging from 0.2 to 3 THz. The THz radiation was focused onto the sample by a pair of parabolic mirrors. The transmitted THz pulse was detected phase-sensitive via electro-optical sampling in an 800 µm thick Zinctelluride crystal by the other part of the amplifier output and autobalanced photodiodes. The beam path of the THz radiation was purged with nitrogen gas to avoid water vapor absorption. Two measurements were performed, one with the pure quartz substrate as the sample ($E_0(t)$) and one with the quartz substrate spin-coated by the perovskite layers ($E_p(t)$). Fourier transformation converted the THz pulses into the frequency domain where the absorption can be calculated using: $\alpha \sim \ln\left(\frac{|E_0(\omega)|^2}{|E_p(\omega)|^2}\right)$.

Optical constants were determined by spectroscopic ellipsometry at 75.48° angle (J.A. Wollam M-2000F).

Characterization of Laser Devices: The perovskite laser samples were optically pumped by a frequency-tripled diode-pumped solid-state laser (PowerChip NanoLaser, TEEM Photonics, France) with $\lambda = 355$ nm, a pulse duration of ≈0.3 ns, and a repetition rate of 1 kHz. The excitation spot had an area of 0.45 mm^2. The excitation density was varied by a neutral density filter wheel. The power of the pump laser was measured with a thermal sensor head (S470C, ThorLabs).

The far field emission characteristics of the DFB laser and VCSEL were recorded by using a sand-blasted glass screen positioned at a distance of about 2–3 cm from the sample surface and a Si CMOS camera (DCC1545M, ThorLabs) with a 25 mm fixed focal length objective.

Supporting Information

Supporting Information is available from the Wiley Online Library or from the author.

Acknowledgements

Conflict of Interest

The authors declare no conflict of interest.

Keywords

cesium lead halide perovskite, distributed feedback lasers, perovskite vertical cavity surface emitting lasers, recrystallization, thermal imprint, thin films

[1] Best Research-Cell Efficiency Chart, https://www.nrel.gov/pv/assets/pdfs/best-research-cell-efficiencies.20190703.pdf (accessed: July 2019).

[2] B. R. Sutherland, E. H. Sargent, Nat. Photonics 2016, 10, 295.

[3] S. D. Stranks, H. J. Snaith, Nat. Nanotechnol. 2015, 10, 391.

[4] S. Adjokatse, H.-H. Fang, M. A. Loi, Mater. Today 2017, 20, 413.

[5] H. Cho, S.-H. Jeong, M.-H. Park, Y.-H. Kim, C. Wolf, C.-L. Lee, J. H. Heo, A. Sadhanala, N. Myoung, S. Yoo, S. H. Im, R. H. Friend, T.-W. Lee, Science 2015, 350, 1222.

[6] W. Xu, Q. Hu, S. Bai, C. Bao, Y. Miao, Z. Yuan, T. Borzda, A. J. Barker, E. Tyukalova, Z. Hu, M. Kawecki, H. Wang, Z. Yan, X. Liu, X. Shi, K. Uvdal, M. Fahlman, W. Zhang, M. Duchamp, J.-M. Liu, A. Petrozza, J. Wang, L.-M. Liu, W. Huang, F. Gao, Nat. Photonics 2019, 13, 418.

[7] K. Lin, J. Xing, L. N. Quan, F. P. G. de Arquer, X. Gong, J. Lu, L. Xie, W. Zhao, D. Zhang, C. Yan, W. Li, X. Liu, Y. Lu, J. Kirman, E. H. Sargent, Q. Xiong, Z. Wei, Nature 2018, 562, 245.

[8] M. Lehnhardt, T. Riedl, T. Weimann, W. Kowalsky, Phys. Rev. B 2010, 81, 165206.

[9] T. Rabe, P. Görrn, M. Lehnhardt, M. Tilgner, T. Riedl, W. Kowalsky, Phys. Rev. Lett. 2009, 102, 137401.

[10] M. Lehnhardt, T. Riedl, U. Scherf, T. Rabe, W. Kowalsky, Org. Electron. 2011, 12, 1346.

[11] P. J. Cegielski, S. Neutzner, C. Porschatis, H. Lerch, J. Bolten, S. Suckow, A. R. S. Kandada, B. Chmielak, A. Petrozza, T. Wahlbrink, A. L. Giesecke, Opt. Express 2017, 25, 13199.

[12] P. J. Cegielski, A. L. Giesecke, S. Neutzner, C. Porschatis, M. Gandini, D. Schall, C. A. R. Perini, J. Bolten, S. Suckow, S. Kataria, B. Chmielak, T. Wahlbrink, A. Petrozza, M. C. Lemme, Nano Lett. 2018, 18, 6915.

[13] T. Langer, A. Kruse, F. A. Ketzer, A. Schwiegel, L. Hoffmann, H. Jönen, H. Bremers, U. Rossow, A. Hangleiter, Phys. Status Solidi C 2011, 8, 2170.

[14] G. Xing, N. Mathews, S. S. Lim, N. Yantara, X. Liu, D. Sabba, M. Grätzel, S. Mhaisalkar, T. C. Sum, Nat. Mater. 2014, 13, 476.

[15] F. Deschler, M. Price, S. Pathak, L. E. Klintberg, D.-D. Jarausch, R. Higler, S. Hüttner, T. Leijtens, S. D. Stranks, H. J. Snaith, M. Atatüre, R. T. Phillips, R. H. Friend, J. Phys. Chem. Lett. 2014, 5, 1421.

[16] B. R. Sutherland, S. Hoogland, M. M. Adachi, C. T. O. Wong, E. H. Sargent, ACS Nano 2014, 8, 10947.

[17] S. Chen, K. Roh, J. Lee, W. K. Chong, Y. Lu, N. Mathews, T. C. Sum, A. Nurmikko, ACS Nano 2016, 10, 3959.

[18] Y. Jia, R. A. Kerner, A. J. Grede, A. N. Brigeman, B. P. Rand, N. C. Giebink, Nano Lett. 2016, 16, 4624.

[19] S. Chen, A. Nurmikko, ACS Photonics 2017, 4, 2486.

[20] N. Pourdavoud, S. Wang, A. Mayer, T. Hu, Y. Chen, A. Marianovich, W. Kowalsky, R. Heiderhoff, H.-C. Scheer, T. Riedl, Adv. Mater. 2017, 29, 1605003.

[21] N. Pourdavoud, A. Mayer, M. Buchmüller, K. Brinkmann, T. Häger, T. Hu, R. Heiderhoff, I. Shutsko, P. Görrn, Y. Chen, H.-C. Scheer, T. Riedl, Adv. Mater. Technol. 2018, 3, 1700253.

[22] B. Conings, J. Drijkoningen, N. Gauquelin, A. Babayigit, J. D'Haen, L. D'Olieslaeger, A. Ethirajan, J. Verbeeck, J. Manca, E. Mosconi, F. D. Angelis, H.-G. Boyen, Adv. Energy Mater. 2015, 5, 1500477.

[23] E. J. Juarez-Perez, Z. Hawash, S. R. Raga, L. K. Ono, Y. Qi, Energy Environ. Sci. 2016, 9, 3406.

[24] M. Kulbak, S. Gupta, N. Kedem, I. Levine, T. Bendikov, G. Hodes, D. Cahen, J. Phys. Chem. Lett. 2016, 7, 167.

[25] A. F. Akbulatov, S. Y. Luchkin, L. A. Frolova, N. N. Dremova, K. L. Gerasimov, I. S. Zhidkov, D. V. Anokhin, E. Z. Kurmaev, K. J. Stevenson, P. A. Troshin, J. Phys. Chem. Lett. 2017, 8, 1211.

[26] S. A. Veldhuis, P. P. Boix, N. Yantara, M. Li, T. C. Sum, N. Mathews, S. G. Mhaisalkar, Adv. Mater. 2016, 28, 6804.

[27] N. Yantara, S. Bhaumik, F. Yan, D. Sabba, H. A. Dewi, N. Mathews, P. P. Boix, H. V. Demir, S. Mhaisalkar, J. Phys. Chem. Lett. 2015, 6, 4360.

[28] M. L. De Giorgi, A. Perulli, N. Yantara, P. P. Boix, M. Anni, J. Phys. Chem. C 2017, 121, 14772.

[29] C. Li, Z. Zang, C. Han, Z. Hu, X. Tang, J. Du, Y. Leng, K. Sun, Nano Energy 2017, 40, 195.

[30] X. Zhang, Z. Jin, J. Zhang, D. Bai, H. Bian, K. Wang, J. Sun, Q. Wang, S. F. Liu, ACS Appl. Mater. Interfaces 2018, 10, 7145.

[31] C. Zhao, W. Tian, J. Liu, Q. Sun, J. Luo, H. Yuan, B. Gai, J. Tang, J. Guo, S. Jin, J. Phys. Chem. Lett. 2019, 10, 2357.

[32] S. Yakunin, L. Protesescu, F. Krieg, M. I. Bodnarchuk, G. Nedelcu, M. Humer, G. De Luca, M. Fiebig, W. Heiss, M. V. Kovalenko, Nat. Commun. 2015, 6, 8056.

[33] S. Kondo, K. Takahashi, T. Nakanish, T. Saito, H. Asada, H. Nakagawa, Curr. Appl. Phys. 2007, 7, 1.

[34] Y. Fu, H. Zhu, C. C. Stoumpos, Q. Ding, J. Wang, M. G. Kanatzidis, X. Zhu, S. Jin, ACS Nano 2016, 10, 7963.

[35] Q. Sun, P. Fassl, D. Becker-Koch, A. Bausch, B. Rivkin, S. Bai, P. E. Hopkinson, H. J. Snaith, Y. Vaynzof, Adv. Energy Mater. 2017, 7, 1700977.

[36] H. Huang, M. I. Bodnarchuk, S. V. Kershaw, M. V. Kovalenko, A. L. Rogach, ACS Energy Lett. 2017, 2, 2071.

[37] M. Cadelano, V. Sarritzu, N. Sestu, D. Marongiu, F. Chen, R. Piras, R. Corpino, C. M. Carbonaro, F. Quochi, M. Saba, A. Mura, G. Bongiovanni, Adv. Opt. Mater. 2015, 3, 1557.

[38] Y. Jia, R. A. Kerner, A. J. Grede, A. N. Brigeman, B. P. Rand, N. C. Giebink, Nano Lett. 2016, 16, 4624.

[39] Z. Xiao, R. A. Kerner, L. Zhao, N. L. Tran, K. M. Lee, T.-W. Koh, G. D. Scholes, B. P. Rand, Nat. Photonics 2017, 11, 108.

[40] J. M. Richter, M. Abdi-Jalebi, A. Sadhanala, M. Tabachnyk, J. P. H. Rivett, L. M. Pazos-Outón, K. C. Gödel, M. Price, F. Deschler, R. H. Friend, Nat. Commun. 2016, 7, 13941.

[41] Y. Rakita, N. Kedem, S. Gupta, A. Sadhanala, V. Kalchenko, M. L. Böhm, M. Kulbak, R. H. Friend, D. Cahen, G. Hodes, Cryst. Growth Des. 2016, 16, 5717.

[42] J. Song, Q. Cui, J. Li, J. Xu, Y. Wang, L. Xu, J. Xue, Y. Dong, T. Tian, H. Sun, H. Zeng, Adv. Opt. Mater. 2017, 5, 1700157.

[43] X. Li, Y. Wu, S. Zhang, B. Cai, Y. Gu, J. Song, H. Zeng, Adv. Funct. Mater. 2016, 26, 2435.

[44] J. I. Pankove, Optical Processes in Semiconductors, Dover, Mineola, NY, USA 1975.

[45] V. D'Innocenzo, A. R. Srimath Kandada, M. De Bastiani, M. Gandini, A. Petrozza, J. Am. Chem. Soc. 2014, 136, 17730.

[46] D. W. de Quilettes, S. M. Vorpahl, S. D. Stranks, H. Nagaoka, G. E. Eperon, M. E. Ziffer, H. J. Snaith, D. S. Ginger, Science 2015, 348, 683.

[47] I. Dursun, M. De Bastiani, B. Turedi, B. Alamer, A. Shkurenko, J. Yin, A. M. El-Zohry, I. Gereige, A. AlSaggaf, O. F. Mohammed, M. Eddaoudi, O. M. Bakr, ChemSusChem 2017, 10, 3746.

[48] G. Li, H. Wang, Z. Zhu, Y. Chang, T. Zhang, Z. Song, Y. Jiang, *Chem. Commun.* **2016**, *52*, 11296.

[49] J. Wang, E. Motaharifar, L. N. S. Murthy, M. Higgins, D. Barrera, T. B. Daunis, Y. Zheng, A. V. Malko, F. Ely, M. Quevedo-Lopez, M. Lee, J. W. P. Hsu, *J. Appl. Phys.* **2019**, *125*, 025706.

[50] H. Shi, X. Zhang, X. Sun, X. Zhang, *Nanoscale* **2018**, *10*, 9892.

[51] O. Yaffe, Y. Guo, L. Z. Tan, D. A. Egger, T. Hull, C. C. Stoumpos, F. Zheng, T. F. Heinz, L. Kronik, M. G. Kanatzidis, J. S. Owen, A. M. Rappe, M. A. Pimenta, L. E. Brus, *Phys. Rev. Lett.* **2017**, *118*, 136001.

[52] X. Tang, Z. Hu, W. Yuan, W. Hu, H. Shao, D. Han, J. Zheng, J. Hao, Z. Zang, J. Du, Y. Leng, L. Fang, M. Zhou, *Adv. Opt. Mater.* **2017**, *5*, 1600788.

[53] X. Zhang, B. Xu, J. Zhang, Y. Gao, Y. Zheng, K. Wang, X. W. Sun, *Adv. Funct. Mater.* **2016**, *26*, 4595.

[54] F. Palazon, S. Dogan, S. Marras, F. Locardi, I. Nelli, P. Rastogi, M. Ferretti, M. Prato, R. Krahne, L. Manna, *J. Phys. Chem. C* **2017**, *121*, 11956.

[55] F. Palazon, F. Di Stasio, S. Lauciello, R. Krahne, M. Prato, L. Manna, *J. Mater. Chem. C* **2016**, *4*, 9179.

[56] T. Haeger, M. Wilmes, R. Heiderhoff, T. Riedl, *J. Phys. Chem. Lett.* **2019**, *10*, 3019.

[57] B. Turedi, K. J. Lee, I. Dursun, B. Alamer, Z. Wu, E. Alarousu, O. F. Mohammed, N. Cho, O. M. Bakr, *J. Phys. Chem. C* **2018**, *122*, 14128.

[58] M. Kasraian, D. Botez, *Appl. Phys. Lett.* **1995**, *67*, 2783.

[59] C.-Y. Huang, C. Zou, C. Mao, K. L. Corp, Y.-C. Yao, Y.-J. Lee, C. W. Schlenker, A. K. Y. Jen, L. Y. Lin, *ACS Photonics* **2017**, *4*, 2281.

[60] Y. Wang, X. Li, V. Nalla, H. Zeng, H. Sun, *Adv. Funct. Mater.* **2017**, *27*, 1605088.

[61] A. Mayer, S. Moellenbeck, K. Dhima, S. Wang, H.-C. Scheer, *J. Vac. Sci. Technol., B: Nanotechnol. Microelectron.: Mater., Process., Meas., Phenom.* **2011**, *29*, 06FC13.

[62] C. Steinberg, K. Dhima, D. Blenskens, A. Mayer, S. Wang, M. Papenheim, H.-C. Scheer, J. Zajadacz, K. Zimmer, *Microelectron. Eng.* **2014**, *123*, 4.

[63] M. Papenheim, C. Steinberg, K. Dhima, S. Wang, H.-C. Scheer, *J. Vac. Sci. Technol., B: Nanotechnol. Microelectron.: Mater., Process., Meas., Phenom.* **2015**, *33*, 06F601.

1903717 (10 of 10)